Fluorescent Nanocomposites: Hollow Silica Microspheres with Embedded Carbon Dots

Asmira Delic,[a] Espen Mariussen,[b] Erik Dobloug Roede,[a] Alexander Krivokapic,[c] Andreas Erbe,[a] Mikael Lindgren,[d] Maria Benelmekki,[a] and Mari-Ann Einarsrud*[a]

Intrinsically fluorescent carbon dots may form the basis for a safer and more accurate sensor technology for digital counting in bioanalytical assays. This work presents a simple and inexpensive synthesis method for producing fluorescent carbon dots embedded in hollow silica particles. Hydrothermal treatment at low temperature (160 °C) of microporous silica particles in presence of urea and citric acid results in fluorescent, microporous and hollow nanocomposites with a surface area of 12 m²/g. High absolute zeta potential (−44 mV) at neutral pH demonstrates the high electrosteric stability of the nanocomposites in aqueous solution. Their fluorescence emission at 445 nm is remarkably stable in aqueous dispersion under a wide pH range (3–12) and in the dried state. The biocompatibility of the composite particles is excellent, as the particles were found to show low genotoxicity at exposures up to 10 µg/cm².

Introduction

Carbon dots (CDs) are a class of discrete carbogenic nanoparticles, with a typical feature size below 10 nm.[1] They are the only carbon nanomaterial with inherent fluorescence and therefore referred to as fluorescent carbon.[2] Their core consists of sp^2/sp^3 hybridized carbon with oxygen and/or nitrogen based functional groups on the surface or at the edges.[1] CDs were identified upon purification of single-walled carbon nanotubes in 2004.[3] Since then, various synthesis routes have been developed. Top-down approaches involve fragmentation of carbon materials such as graphite or carbon nanotubes under harsh physical or chemical conditions.[4] Bottom-up approaches use small organic molecules as the carbon source forming CDs on exposure to heating or microwave pyrolysis.[5] The increasing interest for CDs is particularly due to their tuneable optical response together with biocompatibility, chemical stability, high quantum yield,[5a,6] and low toxicity.[7] In addition, inexpensive and abundant raw materials and simple synthesis routes make them environmentally friendly alternatives to the potentially toxic semiconductor quantum dots, such as CdSe[8] and CdTe.[9] As luminescent materials, CDs are candidates in various application areas, such as chemical sensing,[5a,6, 10] nano-biotechnology,[11] catalysis,[12] light-emitting devices[13] and organic photovoltaic devices.[14]

In the dried solid state CDs aggregate, and the fluorescence is strongly quenched.[15] For this reason, most reports on the synthesis, properties and applications of CDs have dealt with them dispersed in polar solvents, especially water. To expand the application areas, the optical properties of solid state CDs have recently attracted attention. There are two main approaches of conserving the fluorescence of CDs in the dried, solid state. The first is steric hindrance through polymer adsorption, using e.g. PVA,[15] PEG,[5a,16] or PMMA.[13] Hereby, a large enough separation is maintained between the immobilized dots. The second approach is by dispersing and embedding the particles throughout a solid material,[17] thus obtaining a fluorescent composite material.

Porous silica is an excellent host candidate for CDs, as this material has a variety of beneficial properties for multifunctional composites. The size, porosity and surface chemistry of the silica particles can be controlled and a variety of compounds, such as semiconductor quantum dots and metal oxide nanoparticles[18] can be incorporated into the silica. Silica particles are biocompatible[19] and have potential applications as drug delivery vehicles,[20] microreactors and catalyst support[21] and reactors for nanoparticle synthesis.[22]

Synthesis of silica particles with a hollow core and macroporous shell with embedded fluorescent CDs, has to our knowledge not been reported until now. CDs inside mesoporous silica nanoparticles with PEG-modification were prepared by Lai et al.[23] However, the report is unclear on whether the elimination of aggregates of the CDs is due to PEG or the mesoporous structure of silica. Moreover, it was not stated whether the composites were dispersed in a solvent or in dried

[a] A. Delic, E. D. Roede, Prof. Dr. A. Erbe, Dr. M. Benelmekki, Prof. Dr. M.-A. Einarsrud
Department of Materials Science and Engineering
Norwegian University of Science and Technology
Sem Sælands vei 12, NO-7491Trondheim (Norway)
E-mail: mari-ann.einarsrud@ntnu.no
[b] Dr. E. Mariussen
Norwegian Institute for Air Research
NO-2007 Kjeller (Norway)
[c] Dr. A. Krivokapic
Institute for Energy Technology
NO-2007 Kjeller (Norway)
[d] Prof. Dr. M. Lindgren
Department of Physics
Norwegian University of Science and Technology
Høgskoleringen 5, NO-7491Trondheim (Norway)

ChemPlusChem

Full Papers
doi.org/10.1002/cplu.202000801

Chemistry Europe
European Chemical
Societies Publishing

state upon fluorescence measurements. In another study on CDs and mesoporous silica composite,[24] amino-modification was carried out prior to the composite synthesis. The grafted CDs were located only on the outer silica surface. The fluorescence was not measured on the dried particles but for samples dispersed in ethanol.

Here we report on the synthesis, characterisation and toxicity tests of a hollow silica carbon dot composite (silica-CDs), with preserved fluorescence in the dried state and in aqueous dispersions under a wide pH range (from 3 to 12), without any functionalization of the silica, nor the CDs. A simple two-step synthesis route using inexpensive raw materials, was developed. Pristine mesoporous silica was first synthesised by a previously reported, modified Stöber method.[18a] Thereafter, the CDs[5a] were formed in situ by hydrothermal synthesis in a homogeneously dispersed manner throughout the structure of the silica. The hydrothermal process had an additional effect on the mesoporous silica, namely converting it into a macroporous hollow structure. Toxicity tests of the silica-CDs particles with respect to inhalation and release into aquatic environments were conducted in order to qualify them for safe synthesis and potential biomedical applications. The composite particles are shown to have low general toxicity and are proven not to be genotoxic.

Figure 1. a) SEM image of the silica-CDs particles. b) SEM image of FIB sliced silica-CDs particles. The hollow structure is marked with arrows. c) TEM image of the silica-CDs particles. Inset: CDs in the silica structure, marked with rings. d) TEM image of the freestanding CDs.

Results and Discussion

Structure and composition

The morphology of the silica-CDs composite particles is presented in the SEM image in Figure 1a). The partly coarsened particles have a raspberry-like shape, with a rough surface. Their mean diameter is in the range of 500–700 nm and their hollow interior is shown in Figure 1b). These features are prominent in the TEM image in Figure 1c), where the hollow silica sphere with a denser shell is seen. The CDs, homogeneously distributed throughout the inner and outer surface of the silica sphere, are seen in the TEM image. The insert shows that the embedded CDs are approximately 10–15 nm in diameter, i.e. in the same size range as the freestanding CDs in Figure 1d). The size distribution of the latter is presented in Figure S7.

To understand the cause of the hollow structure formation, the pristine silica, i.e. the silica prior to hydrothermal treatment, and the hydrothermally treated silica in water only, i.e. without
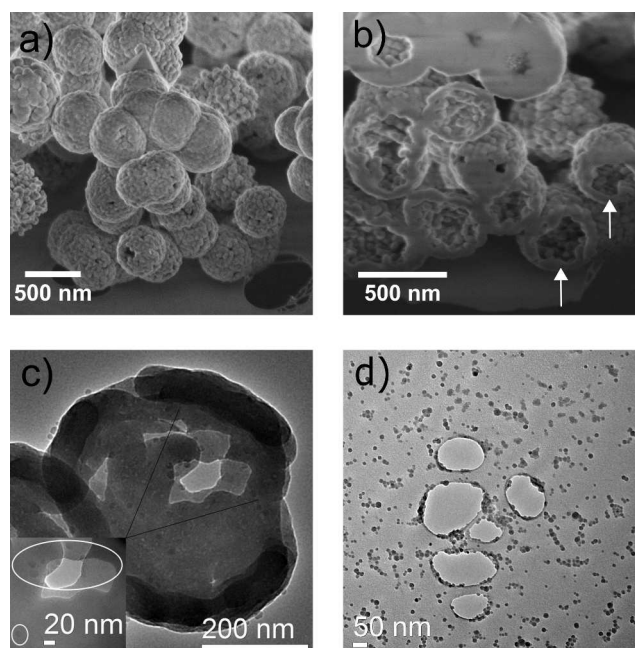
CDs precursors, were examined by electron microscopy. The SEM and TEM images are presented in Figure S8 and S9, respectively. The pristine silica exhibits homogeneous particle density, as marked with arrows on the FIB sliced particles in the insert. The particles are partly coarsened and quasi-monodisperse, with smooth surfaces and diameters in the range 500–700 nm. The pristine silica hydrothermally treated in water only and grounded with a mortar prior to SEM imaging, exhibits the hollow structure. It is obvious that the silica shell is built up by numerous smaller primary particles.

Table 1 gives an overview of the properties of the silica-CDs and pristine silica. The obtained zeta potential for the silica-CDs of −44 mV implies high stability of the particles in aqueous dispersion. Notably, incorporation of CDs in the silica has limited influence on the dispersion stability, as the zeta potential of the silica-CDs composite is similar to that of pristine silica. The surface area and average pore volume of silica after incorporation of the CDs are strongly reduced, showing the

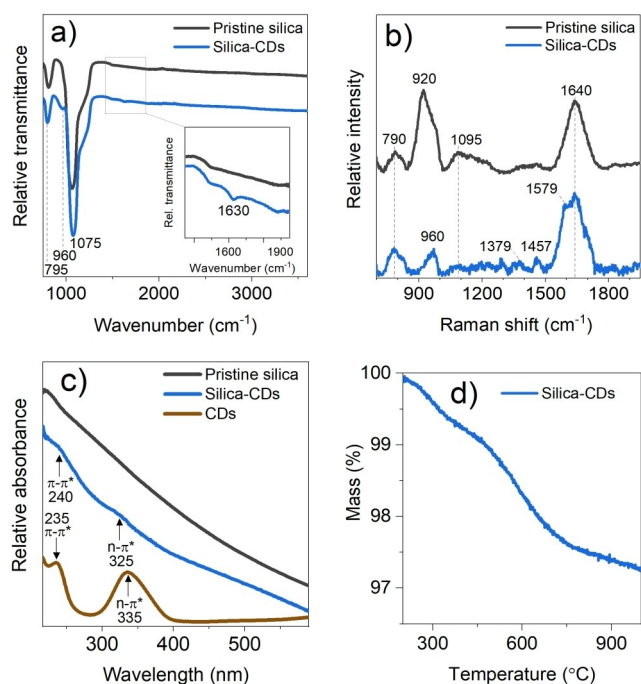| Table 1. Properties of silica-CDs and pristine silica in aqueous dispersion.		
	Silica-CDs	Pristine silica
Zeta potential [mV]	−44±0.4	−50±0.7
Average particle diameter from DLS[a] [nm]	950±10	990±30
pH of dispersion	6.9	6.1
Particle diameter range from TEM [nm]	500–700	500–700
S_{BET}[b] [m²/g]	12±0.3	447±9
V_t[c] [cm³/g]	0.02	0.3
D_{BJH}[d] [Å]	63	24
[a] DLS: Dynamic Light Scattering. [b] S_{BET}: specific surface area obtained by the Brunauer-Emmett-Teller (BET) method. [c] V_t: average pore volume obtained by the Barrett, Joyner and Halenda (BJH) method. [d] D_{BJH}: average pore diameter obtained by BJH analysis of desorption isotherm.		

Figure 2. a) FTIR spectra of dried silica-CDs and pristine silica (data in inset is not in the same scale). b) Raman spectra of silica-CDs and pristine silica. c) UV-Vis spectra of pristine silica, silica-CDs and CDs. d) TG curve of the silica-CDs composite in N_2 atmosphere.

Raman spectra of the pristine silica and the silica-CDs dispersed in water are presented in Figure 2b). Symmetric Si–O–Si stretching mode is apparent at 790 cm^{-1}.[25c] The bands at ~920 cm^{-1} for pristine silica and ~960 cm^{-1} for silica-CDs are assigned to the Si-(OH) stretching.[25c,29] There are three bands in the spectrum of the silica-CDs which do not appear in the spectrum of the pristine silica. The barely visible feature at 1379 cm^{-1} arises due the D band typically ascribed to disordered graphite structures.[5a,30] The band at 1457 cm^{-1} might be assigned to the CH$_2$ scissor mode in the core of CDs.[31] The presence of the embedded CDs is apparent in the G band related to crystalline graphite, observed as a shoulder at 1579 cm^{-1}.[5a,30] Using water as dispersant for the particles gives the OH bending feature at 1640 cm^{-1} for both samples.[32]

UV-Vis absorption spectra of the pristine silica, silica-CDs and freestanding CDs dispersed in water are presented in Figure 2c). Peak positions have been determined by analysing the second derivatives of the spectra. The weak peak in the silica-CDs spectrum at 240 nm is attributed to the π-π^* transition within the aromatic sp^2 domains of the CDs' core.[5a,28a,33] The other weak peak at 325 nm might be ascribed to the n-π^* transition in the surface groups, i.e. the C=O or C–O bonds of the carboxyl (-COOH) surface groups.[28b,34] The corresponding transitions for CDs are at 235 and 335 nm, consistent with the report of Li et al.[5a] The spectrum of the pristine silica exhibits scattering only.

TG analysis in the temperature range 200–1000 °C in N_2 for the silica-CDs sample is shown in Figure 2d). The weight loss is ~3% and can be attributed to the loss of surface groups on the embedded CDs,[5a,35] removal of silanol groups and trace amounts of water from silica.[36]

Photoluminescence

PL emission spectra of the silica-CDs and the freestanding CDs with progressively longer excitation wavelengths are displayed in Figure 3a) and b), respectively. An excitation-independent PL was observed for both samples, with the emission peak position at 440 nm for all excitation wavelengths. The emission was
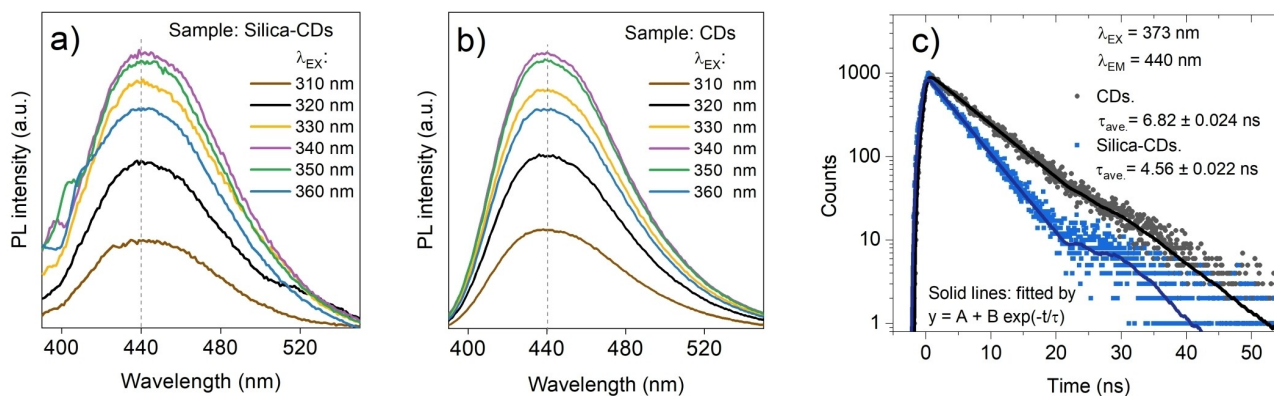
removal of a large fraction of the mesoporosity developed by using the cetyltrimethylammonium bromide during the synthesis of pristine silica.

FTIR spectra in Figure 2a) of the pristine silica and silica-CDs dried at 60 °C in vacuum, exhibit symmetric stretching vibrations of Si–O–Si at 795 cm^{-1}[25] and asymmetric stretching vibration of Si–O–Si at 1075 cm^{-1}.[25a,26] The spectrum of the silica-CDs has a shoulder at 960 cm^{-1} assigned to the Si–(OH) stretching vibrations.[27] The band at 1630 cm^{-1} for the silica-CDs in the insert might be C=O stretching of the surface groups on the embedded CDs[28] and/or bending modes of residual adsorbed water molecules in the porous structure of silica.[25a,26]

Figure 3. a) and b) PL emission spectra of silica-CDs and CDs, respectively, in aqueous solution at progressively longer excitation wavelengths from 310 to 360 nm in 10 nm increment. c) PL decay curves of silica-CDs and CDs fitted with single-exponential function.
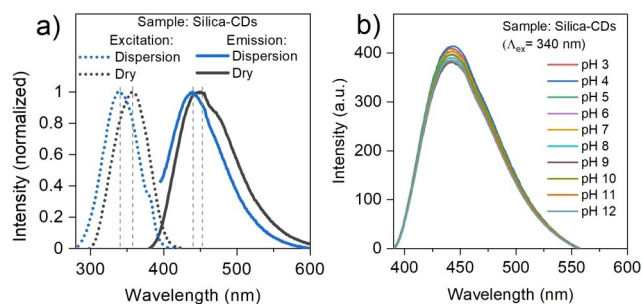
ChemPlusChem

Full Papers
doi.org/10.1002/cplu.202000801

**Chemistry
Europe**
European Chemical
Societies Publishing

Figure 4. a) Excitation and emission spectra for silica-CDs in aqueous dispersion and dried in vacuum at 60 °C. Dotted blue spectrum: $\lambda_{EM} = 440$ nm, dotted grey spectrum: $\lambda_{EM} = 450$ nm, solid blue spectrum: $\lambda_{EX} = 340$ nm and solid grey spectrum: $\lambda_{EX} = 360$ nm. b) Emission spectra for silica-CD in buffers of pH 3–12.

Figure 6. DNA damage in RTgill-w1 cells measured by the comet assay after exposure to the silica-CDs in mass per area, a) for 3 h and b) for 24 h. Relative amount of DNA in the comet tail represents the amount of DNA strand breaks (SBs). Net Fpg represents the modified version of the comet assay applying the endonuclease for detection of oxidized purines and is a measure of the level of oxidative stress. Results are presented as mean DNA tail intensity ($\pm$ SD) of 3 independent experiments performed in triplicate.

largest for the 340 nm excitation wavelength. These results are in agreement with the findings of Li et al.[5a] for CDs synthesised at 160 °C. Time-correlated single photon counting was employed to investigate fluorescence decay times (Figure 3c). Good deconvolution fits of the PL decay curves were obtained by using a single-exponential function (solid lines in Figure 3c), resulting in an average lifetime of 6.8 and 4.6 ns for CDs and silica-CDs, respectively. The faster decay time of the embedded CDs indicate that they are to some extent altered when bonded to the silica structure.

To further examine the optical properties of the silica-CDs, the PL characteristics were compared between the sample in dried state, in aqueous dispersion and dispersion in buffers with pH 3–12. Normalised excitation and emission spectra of silica-CDs in aqueous dispersion and dried silica-CDs are presented in Figure 4a). The silica-CDs dispersed in water have the maximum excitation intensity at 340 nm. The dried silica-CDs composite also exhibits PL, but with the maximum excitation peak position redshifted to 360 nm and maximum emission peak redshifted to 450 nm, compared to the sample in aqueous dispersion.

The PL spectra of silica-CDs dispersed in buffers at pH 3–12, at excitation wavelength 340 nm are presented in Figure 4b). To evaluate the relative intensity, the integrated PL intensities are plotted as a function of buffer solution pH in Figure 5a). The embedded CDs show higher PL intensity under acidic con-
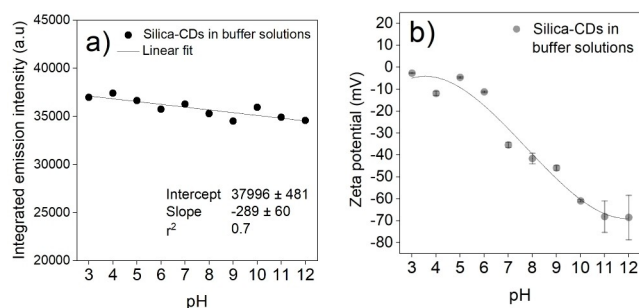
ditions. Nevertheless, the decrease in PL intensity towards the alkaline regime is small and approximately linear, evident from the slope of the regression line.

Zeta poztential values of the silica-CDs in buffer solutions of pH 3–12 are shown in Figure 5b). The absolute zeta potential value increases with increasing pH, which is consistent with previous reports on Stöber silica particles.[37]

Toxicity

The comet assay showed no significant genotoxic effects on the cells when exposed to the silica-CDs (Figure 6, S1 and S2). A significant reduction in cell viability with more than 80 % reduction of cell viability (Figure S3–S5) was only observed on the rainbow trout gill cells at the two highest exposure concentrations only (50 and 100 µg/cm^2). The CTA results show that the particles were cytotoxic to the cells at high concentrations (25 and 50 µg/cm^2), particularly in the initiation assay, in which a very low number of cells are exposed (Figure S6). The particles induced an increase in cell transformation in the promotion assay, indicating a tumour promoting effect (Figure 7).

Discussion

Two processes occur during the hydrothermal treatment of silica particles in the presence of urea and citric acid, as precursors for CDs. One is the altering of the silica particle morphology, and the other is the formation of CDs. Due to the hydrothermal treatment, the initial uniform surface and homogeneous density of the pristine silica (Figure S8) changes to raspberry-like surface and hollow interior (Figure 1) accompanied by reduction of mesoporosity and increased pore diameter for the composite particles (Table 1). This process can be explained by the inside-out Ostwald ripening mechanism, taking place due to dissolution of silica at elevated temperatures in aqueous solution.[38] Each silica sphere is constituted by smaller particles, which dissolve more in the inner part of

Figure 5. a) Integrated PL emission intensities of silica-CDs in buffer solutions at pH 3–12 at excitation wavelength 340 nm. b) Zeta potential for silica-CDs in buffer solutions of pH 3–12. The line serves as a guide to the eye for the data points.
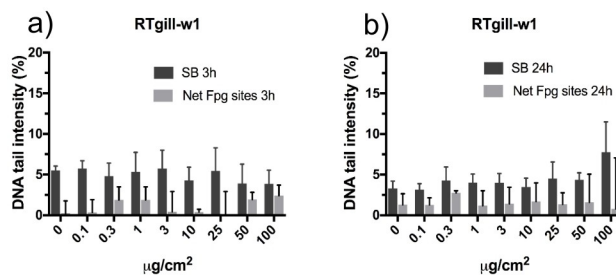
ChemPlusChem

Full Papers
doi.org/10.1002/cplu.202000801

Chemistry
Europe
European Chemical
Societies Publishing

the sphere, presumably because they are packed more loosely than those in the shell. Our results demonstrate that this process is independent of the presence of citric acid and urea under the hydrothermal treatment of silica (Figure S9).

The porosity, and hence high surface area of the pristine mesoporous silica facilitates the incorporation of the CDs precursors. Under hydrothermal treatment, formation of embedded CDs in the inner and outer structure of the silica particles takes place. The CDs are randomly distributed throughout the amorphous silica matrix. The pores of the pristine silica do not dictate the size of the resulting CDs. The average pore size was ~2.4 nm (Table 1), whilst the size of the embedded CDs is 10–15 nm in diameter (Figure 1c)), i.e. in the same size range as the freestanding CDs (Figure 1d) and S7).

The Raman spectra show that the core of the embedded CDs in silica consists of both amorphous and crystalline carbon phases, as previously reported.[5a] FTIR spectrum of the silica-CDs composite indicates that the embedded CDs have carboxyl groups on the surface. The UV-Vis spectrum of the silica-CDs composite has weak and asymmetric absorption peaks, probably due to scattering from the silica particles, which dominate the composition. The peak at 325 nm (n-π*) is typical for oxygen-based surface groups on CDs.[5a,28a] The presence of the CDs' surface groups was confirmed by the TG measurement. These results indicate that dehydration and condensation reactions between silanols on silica and carboxyl and hydroxy groups on the CDs might have occurred to yield CDs bonded to the silica structure.

The optical properties are slightly altered when the CDs are embedded in silica, and when the composite particles are dried. It is well known that the PL of many fluorophores is dependent on the surrounding local environment,[39] and our results show that this is also the case for the silica-CDs. Nevertheless, the PL emission of the composite particles is preserved even after drying at 60°C under vacuum. The dried sample shows a small redshift in the excitation and emission spectra, compared to the sample in aqueous dispersion. No water is present in the dried sample, as evident from the FTIR spectrum. It is therefore plausible to assume that the dispersion and immobilization of the CDs throughout the silica structure offers an alternative to avoid agglomeration and thereby also PL quenching.[17] The PL dependency on pH shows that the embedded CDs have the highest PL intensity under acidic conditions. This behaviour can be explained by the protonation–deprotonation of the acidic carboxyl surface groups on the CDs.[40] However, the overall influence of pH is small. The silica matrix seems to stabilize the PL intensity of the CDs at different pH values, as the PL intensity as a function of pH for freestanding CDs is reported to be very low under acidic conditions.[5a] The surface charge is primarily determined by the surface properties of silica, i.e. the CDs have no apparent influence, as evident from the zeta potential measurements of the composite particles.

The toxicity of the silica-CDs is in general low on the human lung cells and fish cells. Some cytotoxicity was observed on the gill cell with a 30% reduction in viability after 24 h exposure with the two highest concentrations, but this had no significant influence on the comet assay. Reports about genotoxicity of

amorphous silica particles are mixed, but in general they are shown to have a low genotoxic potential, particularly at noncytotoxic concentrations.[41] The toxicity of inert nanomaterials, such as silica particles, are linked to size and surface reactivity. In a study by Brown et al.[42] the smaller sized (50 nm) silica nanoparticles showed more DNA damage compared to their larger (200 nm) counterparts. The surface reactivity of particles is influenced by the composition of the surrounding fluid. It has been suggested that biological fluids which have a high content of proteins, such as serum albumin, will reduce the surface reactivity of the particles followed by reduced toxicity due to adsorption on the particle surface.[41]

The CTA, however, revealed that the composite has a non-genotoxic carcinogenic potential as shown in the promotion assay, indicating a tumour promoting effect. The effect was induced at relatively high concentration, which were cytotoxic, but agrees with recent experiments by Fontana et al.[43] who investigated four different amorphous non-genotoxic silica particles with the similar assay; two pyrogenic and two precipitated silica materials. As in our study, they did not observe any effect in the initiation assay, which is indicative of a genotoxic carcinogen. The mechanism of the tumour promoting effect is not known, but unlike initiators, promoters do not covalently bind to DNA or macromolecules within the cell. Many promoters bind specifically to receptors on the cell surface in order to affect intracellular pathways that lead to increased cell proliferation. Our finding, in addition to the recent work by Fontana et al.,[43] should merit further investigation on the potential of silica particles to have a tumour-promoter activity, particularly under high exposure.

The composite silica-CDs particles with hollow core, microporous shell structure and low toxicity might conceptually be ideal for drug storage and release systems.[20] The fluorescence is highly sensitive to the concentration of the particles, and a drug dosage can thereby be controlled precisely. Other potential application areas are within bioanalytical assays[44] and as microreactors.[21]
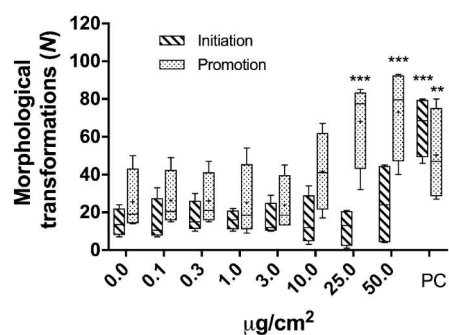

Figure 7. Number of morphological transformations (foci) of the Bhas42 cells after exposure to the silica-CD indicating tumour promoting effects at high concentrations. The results are shown as Box and Whiskers plot from four independent experiments (max and min, 25th and 75th percentile, median and mean (+)). Asterisks indicate significant different effects compared to control analysed by one-way ANOVA followed by Dunnet post test (**$p < 0.01$, ***$p < 0.001$).

ChemPlusChem

Full Papers
doi.org/10.1002/cplu.202000801

Chemistry Europe
European Chemical
Societies Publishing

Conclusion

A simple hydrothermal synthesis route was developed to produce fluorescent hollow silica-CDs composite particles. The method is an efficient way to disperse and embed CDs into a solid, porous material, and thereby preserve the PL. The composite exhibits PL in aqueous dispersion under a wide pH range, and in the dried state. The particles had low general toxicity and were proven not to be genotoxic. High concentrations of the particles indicated non-genotoxic carcinogenic potential, in line with previous findings on particulate matter of silica. The biocompatible porous silica-CDs composite has a potential application in bioanalytical assays or drug carriers where PL can be used as a digital counting method.

Experimental Section

Synthesis of the materials

Freestanding CDs: The synthesis method is previously reported by Li et al.[5a] In brief, citric acid (1 g, VWR Chemicals, $\geq 99\%$) and urea (0.5 g, VWR Chemicals, $\geq 99.5\%$) were dissolved in Milli-Q® water (25 mL). After transfer to a PTFE-lined autoclave (Parr Instrument Company, Moline, Illinois, USA), the mixture was heated at 160 °C for 6 h, followed by natural cooling. The product was transferred into a dialysis tubing, 1 kD MWCO, 38 mm flat-width (Repligen, Waltham, Massachusetts, USA) and dialyzed against Milli-Q® water for 24 h.

Mesoporous silica: the synthesis was based on a previously reported method.[18a] Cetyltrimethylammonium bromide (0.112 g, VWR Chemicals, $\geq 99\%$) was added to a mixture of Milli-Q® water (14 mL), ethanol (60 mL, VWR Chemicals, 99,95%) and ammonia solution (5 mL, VWR Chemicals, 25%). Tetraethyl orthosilicate (800 μL, Sigma-Aldrich, $\geq 99.99\%$) was added quickly, and the solution was left for aging at room temperature under continuous stirring for 44 h. The obtained white powder precipitate was centrifuged and washed with Milli-Q® water three times. The surfactant was removed by calcination in air at 550 °C for 6 h, with a heating rate of 1 °C/min, to obtain the pristine mesoporous silica.

The silica-CDs composite: citric acid (1 g, VWR Chemicals, $\geq 99\%$) and urea (0.5 g, VWR Chemicals, $\geq 99.5\%$) were dissolved in Milli-Q® water (25 mL).[5a] Pristine silica (40 mg) was then added under stirring. After transfer to a PTFE-lined autoclave (Parr Instrument Company, Moline, Illinois, USA), the mixture was heated at 160 °C for 6 h, followed by natural cooling. The resulting silica-CDs composite particles were collected by centrifugation at 5000 rpm for 30 min. The composite particles were washed with Milli-Q® water and centrifuged at 5000 rpm for 30 min. This step was repeated three times. The silica particles were subsequently washed with Milli-Q® water through a Vivaspin Ultrafiltration unit (30 000 MWCO) (Sartorius, Göttingen, Germany), to remove residual CDs, until the supernatant had no fluorescence by visual inspection under UV lamp of 366 nm.

For further characterisation, one part of the silica-CDs sample was re-dispersed in Milli-Q® water or buffer solutions with pH 3–12 (VWR Chemicals), and another part dried in vacuum at 60 °C for 24 h. A parallel sample of the pristine silica (40 mg) was dispersed in Milli-Q® water (25 mL) and treated hydrothermally 160 °C for 6 h. After natural cooling, the silica was collected by centrifugation at 5000 rpm for 30 min.

Characterisation

Transmission electron microscopy (TEM) imaging was performed on a JEM-2100 200 kV electron microscope (Jeol, Tokyo, Japan). The TEM images were processed with DigitalMicrographH (Gatan Inc. version 3.32). A Helios G4 DualBeam™ (Thermo Scientific™, Hillsboro, Oregon, USA) was used to cut the particles with focused ion beam (FIB) and to record scanning electron microscopy (SEM) images. The TEM and SEM samples were prepared by deposition of the aqueous dispersions of the particles onto holey carbon film on Cu grids (Lacey, Electron Microscopy Sciences). After deposition, the grids were left to dry at ambient temperature for 1 h.

Thermogravimetry (TG) measurements were carried out in a STA449 F3 Jupiter (NETZSCH, Selb, Germany). The sample was placed in an alumina crucible and heated up to 1000 °C at a rate of 10 °C/min in N_2.

Fourier-transform infrared (FTIR) spectra were recorded with a VERTEX 80v vacuum spectrometer (Bruker Optics, Ettlingen, Germany), equipped with a Platinum ATR diamond sampling accessory. The samples analysed were dried powders. 128 scans with a resolution of 4 cm^{-1} were acquired for each FTIR spectrum. Raman spectroscopy measurements were performed on an alpha300 R (WITec, Ulm, Germany) using the 532 nm wavelength incident light of a frequency-doubled solid-state Nd-YAG laser. Laser power was set to 66 mW. The samples dispersed in water were placed on Menzel microscope coverslips and a Zeiss EC Epiplan 50x objective was used. The grating was set to 600 lines/mm. The integration time was 30 s, with 10 accumulations.

Surface area, pore size, and pore volume were obtained by nitrogen adsorption using a Tristar 3000 Analyser (Micromeritics Instrument Corporation, Norcross, Georgia, USA). Brunauer, Emmett, Teller (BET) method was used to calculate the specific surface area, and the Barret, Joyner, Halenda (BJH) algorithm was used to determine the pore diameter and volume. Prior to the nitrogen adsorption measurements, the samples were degassed under vacuum at 250 °C for 24 h.

Zetasizer Nano ZS instrument (Malvern Panalytical Ltd, Malvern, UK) was used to obtain the zeta potential and hydrodynamic particle diameter, in three parallel measurements for particles suspended in Milli-Q® water and buffer solutions with pH 3–12 at 25 °C. The reported zeta potential and hydrodynamic particle diameter are the mean average of the three parallel measurements, with population standard deviation.

UV-Vis spectra were measured with an Evolution 220 UV-Visible spectrophotometer (Thermo Fisher Scientific, Shanghai, China) equipped with Xenon flash lamp and dual silicon photodiodes detector. Steady state fluorescence measurements were carried out using a PTI Quantamaster 8075-22 (Horiba Scientific, Kyoto, Japan) equipped with Double Mono 300 spectrometer chambers for both excitation and emission. As light source the OB-75X (75 W Xenon arc lamp) was used. A Hamamatsu R928 PMT (Hamamatsu, Japan) was used for detection in the range 185–950 nm. Data acquisition and basic data-handling was carried out with the Felix Data Analysis software. For PL measurements on samples dispersed in water and buffers, plastic disposable UV-transparent cuvettes (Brand) with 10 mm light path were used. The dried sample was pressed between two Menzel microscope coverslips and mounted on a custom-made sample holder. Time resolved PL decay measurements were recorded with an IBH time-correlated single photon counting system using deconvolution to fit the decays. A laser diode operating at 373 nm was used as excitation source, and the emission was recorded at 440 nm. Details of the setup and procedures were previously reported by Glimsdal et al.[45]

ChemPlusChem

Full Papers
doi.org/10.1002/cplu.202000801

Chemistry Europe
European Chemical
Societies Publishing

Toxicity testing

The toxicity of the silica-CDs was tested on two different assays; the comet assay and the cell transformation assay (CTA). The assays were performed as previously reported in detail,[46] and in Supporting Information. The comet assay is a common test for genotoxicity of nanomaterials where DNA damage on single cells is detected.[46] The basic principle of the comet assay is to embed exposed single cells in agarose on a microscope slide, lyse the cells with a detergent and subject the cells to electrophoresis at high pH. The electrophoresis results in structures resembling comets of which the intensity of the comet tail relative to the nuclear head reflects the number of DNA strand breaks (SBs). The comet assay was performed on a human alveolar lung cell line as a model for human toxicity, and gill and liver cell lines from rainbow trout were used as models for ecotoxicity. Both a standard comet assay measuring single- and double-strand breaks and a modified version of the assay with use of the lesion-specific enzyme formamidopyrimidine DNA glycosylase (Fpg) that detect specific DNA lesions, were applied. The CTA is a promising test for predicting chemical and nanomaterial induced carcinogenicity in vitro.[47] In particular, the CTA assay has been proven valuable for the identification of non-genotoxic carcinogens. The basic principle of the CTA assay is to measure morphological transformation of Bhas42 cells derived from single cells. The cell transformation is visualized in a stereo microscope as so-called foci, which are local accumulations of cells of characteristic shapes and forms, which differs from non-transformed cells. The CTA assay is divided in two separate experiments. An initiation and a promotion assay, which aim to predict tumour-initiating and tumour-promoting activity of a substance respectively. As an integral part of the above-mentioned assays, the cytotoxicity of the silica-CDS was assessed with the alamarBlue assay, which is based on a non-toxic dye, resazurin, that yields colorimetric change and a fluorescent signal in response to metabolic activity.[46]

Conflict of Interest

The authors declare no conflict of interest.

Keywords: biocompatibility · carbon dots · fluorescence · Ostwald ripening · silica

[1] S. Zhu, Y. Song, X. Zhao, J. Shao, J. Zhang, B. Yang, *Nano Res.* **2015**, *8*, 355–381.

[2] H. Li, Z. Kang, Y. Liu, S.-T. Lee, *J. Mater. Chem.* **2012**, *22*, 24230–24253.

[3] X. Xu, R. Ray, Y. Gu, H. J. Ploehn, L. Gearheart, K. Raker, W. A. Scrivens, *J. Am. Chem. Soc.* **2004**, *126*, 12736–12737.

[4] a) Y.-P. Sun, B. Zhou, Y. Lin, W. Wang, K. A. S. Fernando, P. Pathak, M. J. Meziani, B. A. Harruff, X. Wang, H. Wang, P. G. Luo, H. Yang, M. E. Kose, B. Chen, L. M. Veca, S.-Y. Xie, *J. Am. Chem. Soc.* **2006**, *128*, 7756–7757; b) Z.-A. Qiao, Y. Wang, Y. Gao, H. Li, T. Dai, Y. Liu, Q. Huo, *Chem. Commun.* **2010**, *46*, 8812–8814; c) D. B. Shinde, V. K. Pillai, *Chem. Eur. J.* **2012**, *18*, 12522–12528.

[5] a) X. Li, S. Zhang, S. A. Kulinich, Y. Liu, H. Zeng, *Sci. Rep.* **2014**, *4*, 4976; b) Z.-C. Yang, M. Wang, A. M. Yong, S. Y. Wong, X.-H. Zhang, H. Tan, A. Y. Chang, X. Li, J. Wang, *Chem. Commun.* **2011**, *47*, 11615–11617; c) H. Zhu, X. Wang, Y. Li, Z. Wang, F. Yang, X. Yang, *Chem. Commun.* **2009**, 5118–5120.

[6] S. Zhu, Q. Meng, L. Wang, J. Zhang, Y. Song, H. Jin, K. Zhang, H. Sun, H. Wang, B. Yang, *Angew. Chem. Int. Ed.* **2013**, *52*, 3953–3957.

[7] T. Huiquan, Y. Kai, M. Zhen, W. Jianmei, Z. Youjiu, K. Zhenhui, L. Zhuang, *Small* **2012**, *8*, 281–290.

[8] A. M. Derfus, W. C. W. Chan, S. N. Bhatia, *Nano Lett.* **2004**, *4*, 11–18.

[9] J. Lovrić, S. J. Cho, F. M. Winnik, D. Maysinger, *Chem. Biol.* **2005**, *12*, 1227–1234.

[10] Y. Hou, Q. Lu, J. Deng, H. Li, Y. Zhang, *Anal. Chim. Acta* **2015**, *866*, 69–74.

[11] a) S. Nandi, R. Malishev, K. Parambath Kootery, Y. Mirsky, S. Kolusheva, R. Jelinek, *Chem. Commun.* **2014**, *50*, 10299–10302; b) C. Liu, P. Zhang, X. Zhai, F. Tian, W. Li, J. Yang, Y. Liu, H. Wang, W. Wang, W. Liu, *Biomaterials* **2012**, *33*, 3604–3613; c) L. Wang, X. Wang, A. Bhirde, J. Cao, Y. Zeng, X. Huang, Y. Sun, G. Liu, X. Chen, *Adv. Healthcare Mater.* **2014**, *3*, 1203–1209; d) Y. Xu, M. Wu, Y. Liu, X.-Z. Feng, X.-B. Yin, X.-W. He, Y.-K. Zhang, *Chem. Eur. J.* **2013**, *19*, 2276–2283; e) C. Fowley, B. McCaughan, A. Devlin, I. Yildiz, F. M. Raymo, J. F. Callan, *Chem. Commun.* **2012**, *48*, 9361–9363.

[12] a) H. Li, X. He, Z. Kang, H. Huang, Y. Liu, J. Liu, S. Lian, C. H. A. Tsang, X. Yang, S.-T. Lee, *Angew. Chem. Int. Ed.* **2010**, *49*, 4430–4434; *Angew. Chem.* **2010**, *122*, 4532–4536; b) Z. Ma, H. Ming, H. Huang, Y. Liu, Z. Kang, *New J. Chem.* **2012**, *36*, 861–864.

[13] W. Kwon, S. Do, J. Lee, S. Hwang, J. K. Kim, S.-W. Rhee, *Chem. Mater.* **2013**, *25*, 1893–1899.

[14] V. Gupta, N. Chaudhary, R. Srivastava, G. D. Sharma, R. Bhardwaj, S. Chand, *J. Am. Chem. Soc.* **2011**, *133*, 9960–9963.

[15] Y. Chen, M. Zheng, Y. Xiao, H. Dong, H. Zhang, J. Zhuang, H. Hu, B. Lei, Y. Liu, *Adv. Mater.* **2016**, *28*, 312–318.

[16] P. Long, Y. Feng, Y. Li, C. Cao, S. Li, H. An, C. Qin, J. Han, W. Feng, *ACS Appl. Mater. Interfaces* **2017**, *9*, 37981–37990.

[17] F. Messina, L. Sciortino, G. Buscarino, S. Agnello, F. Gelardi, M. Cannas, *Mater. Today: Proc.* **2016**, *3*, S258–S265.

[18] a) M. Benelmekki, E. Xuriguera, C. Caparros, E. Rodríguez-Carmona, R. Mendoza, J. L. Corchero, S. Lanceros-Mendez, L. M. Martinez, *J. Colloid Interface Sci.* **2012**, *365*, 156–162; b) J. Kim, J. E. Lee, J. Lee, J. H. Yu, B. C. Kim, K. An, Y. Hwang, C.-H. Shin, J.-G. Park, J. Kim, T. Hyeon, *J. Am. Chem. Soc.* **2006**, *128*, 688–689; c) I. Gorelikov, N. Matsuura, *Nano Lett.* **2008**, *8*, 369–373; d) Y.-S. Lin, S.-H. Wu, Y. Hung, Y.-H. Chou, C. Chang, M.-L. Lin, C.-P. Tsai, C.-Y. Mou, *Chem. Mater.* **2006**, *18*, 5170–5172.

[19] a) J. Lu, M. Liong, Z. Li, J. I. Zink, F. Tamanoi, *Small* **2010**, *6*, 1794–1805; b) F. Tang, L. Li, D. Chen, *Adv. Mater.* **2012**, *24*, 1504–1534.

[20] J. Xie, C. Yang, Q. Liu, J. Li, R. Liang, C. Shen, Y. Zhang, K. Wang, L. Liu, K. Shezad, M. Sullivan, Y. Xu, G. Shen, J. Tao, J. Zhu, Z. Zhang, *Small* **2017**, *13*, 1701741.

[21] Y. Yamada, M. Mizutani, T. Nakamura, K. Yano, *Chem. Mater.* **2010**, *22*, 1695–1703.

[22] S. Ding, J. S. Chen, G. Qi, X. Duan, Z. Wang, E. P. Giannelis, L. A. Archer, X. W. Lou, *J. Am. Chem. Soc.* **2011**, *133*, 21–23.

[23] C.-W. Lai, Y.-H. Hsiao, Y.-K. Peng, P.-T. Chou, *J. Mater. Chem.* **2012**, *22*, 14403–14409.

[24] S. Zhao, S. Sun, K. Jiang, Y. Wang, Y. Liu, S. Wu, Z. Li, Q. Shu, H. Lin, *Nano-Micro Lett.* **2019**, *11*, 32.

[25] a) H. Sanaeishoar, M. Sabbaghan, F. Mohave, *Microporous Mesoporous Mater.* **2015**, *217*, 219–224; b) P. Innocenzi, *J. Non-Cryst. Solids* **2003**, *316*, 309–319; c) C. J. Brinker, G. W. Scherer in *Sol-Gel Science* (Eds.: C. J. Brinker, G. W. Scherer), Academic Press, San Diego, **1990**, pp. 514–615.

[26] V. S. A. Beganskiene, M. Kurtinattiene, R. Juskenas, A. Kareiva, *Mat. Sci.* **2004**, *10*, 287–290.

[27] R. M. Almeida, C. G. Pantano, *J. Appl. Phys.* **1990**, *68*, 4225–4232.

[28] a) Z. Yang, M. Xu, Y. Liu, F. He, F. Gao, Y. Su, H. Wei, Y. Zhang, *Nanoscale* **2014**, *6*, 1890–1895; b) Y. Zhao, X. Liu, Y. Yang, L. Kang, Z. Yang, W. Liu, L. Chen, *Fullerenes Nanotubes Carbon Nanostruct.* **2015**, *23*, 922–929.

[29] A. Alessi, S. Agnello, G. Buscarino, F. M. Gelardi, *J. Raman Spectrosc.* **2013**, *44*, 810–816.

[30] M. Zhang, L. Bai, W. Shang, W. Xie, H. Ma, Y. Fu, D. Fang, H. Sun, L. Fan, M. Han, C. Liu, S. Yang, *J. Mater. Chem.* **2012**, *22*, 7461–7467.

[31] J. Filik, J. Harvey, N. Allan, P. May, J. Dahl, S. Liu, R. Carlson, *Phys. Rev. B* **2006**, *74*.

[32] D. M. Carey, G. M. Korenowski, *J. Chem. Phys.* **1998**, *108*, 2669–2675.

[33] D. Pan, J. Zhang, Z. Li, M. Wu, *Adv. Mater.* **2010**, *22*, 734–738.

[34] A. N. Emam, S. A. Loutfy, A. A. Mostafa, H. Awad, M. B. Mohamed, *RSC Adv.* **2017**, *7*, 23502–23514.

[35] Y. Yang, X. Ji, M. Jing, H. Hou, Y. Zhu, L. Fang, X. Yang, Q. Chen, C. E. Banks, *J. Mater. Chem. A* **2015**, *3*, 5648–5655.

[36] L. Peng, W. Qisui, L. Xi, Z. Chaocan, *Colloids Surf. A* **2009**, *334*, 112–115.

[37] P. Wilhelm, D. Stephan, *J. Colloid Interface Sci.* **2006**, *293*, 88–92.

[38] a) X. W. Lou, Y. Wang, C. Yuan, J. Y. Lee, L. A. Archer, *Adv. Mater.* **2006**, *18*, 2325–2329; b) L. Zhang, H. Wang, *J. Phys. Chem. C* **2011**, *115*, 18479–18485; c) L. Zhang, H. Wang, *ACS Nano* **2011**, *5*, 3257–3267; d) Q. Yu, P. Wang, S. Hu, J. Hui, J. Zhuang, X. Wang, *Langmuir* **2011**, *27*, 7185–7191.

[39] a) L. Sciortino, F. Messina, G. Buscarino, S. Agnello, M. Cannas, F. M. Gelardi, *J. Nanopart. Res.* **2017**, *19*, 228; b) J. Schneider, C. J. Reckmeier, Y. Xiong, M. von Seckendorff, A. S. Susha, P. Kasák, A. L. Rogach, *J. Phys. Chem. C* **2017**, *121*, 2014–2022.

[40] T. Wang, G. Chen, L. Li, Y. Wu, *Sensors* **2019**, *19*, 3801.

[41] M. Yazdimamaghani, P. J. Moos, M. A. Dobrovolskaia, H. Ghandehari, *Nanomedicine* **2019**, *16*, 106–125.

[42] D. M. Brown, J. Varet, H. Johnston, A. Chrystie, V. Stone, *J. Nanopart. Res.* **2015**, *17*, 410.

[43] C. Fontana, A. Kirsch, C. Seidel, L. Marpeaux, C. Darne, L. Gaté, A. Remy, Y. Guichard, *Mutat. Res. Genet. Toxicol. Environ. Mutagen.* **2017**, *823*, 22–27.

[44] L. M. Rossi, L. Shi, F. H. Quina, Z. Rosenzweig, *Langmuir* **2005**, *21*, 4277–4280.

[45] E. Glimsdal, I. Dragland, M. Carlsson, B. Eliasson, T. B. Melø, M. Lindgren, *J. Phys. Chem. A* **2009**, *113*, 3311–3320.

[46] M. Dusinska, E. Mariussen, E. Runden-Pran, A. M. Hudecova, E. Elje, A. Kazimirova, N. El Yamani, N. Dommershausen, J. Tharmann, D. Fieblinger, F. Herzberg, A. Luch, A. Haase, *Methods Mol. Biol.* **2019**, *1894*, 83–122.

[47] K. Sasaki, M. Umeda, A. Sakai, S. Yamazaki, N. Tanaka, *Environ. Carcinog. Ecotoxicol. Rev.* **2015**, *33*, 1–35.